2020

Human ferroportin mediates proton-coupled active transport of iron

Shuang Li

Yihu Yang

Weikai Li

Human ferroportin mediates proton-coupled active transport of iron

Shuang Li,* Yihu Yang,* and Weikai Li

Department of Biochemistry and Molecular Biophysics, Washington University School of Medicine, St. Louis, MO

Key Points

- Active iron export by ferroportin can be driven by proton gradient and charge potential.

- Mutagenesis analysis suggests that the iron translocation site is at the pore region of ferroportin.

As the sole iron exporter in humans, ferroportin controls systemic iron homeostasis through exporting iron into the blood plasma. The molecular mechanism of how ferroportin exports iron under various physiological settings remains unclear. Here we found that purified ferroportin incorporated into liposomes preferentially transports Fe^{2+} and exhibits lower affinities of transporting other divalent metal ions. The iron transport by ferroportin is facilitated by downhill proton gradients at the same direction. Human ferroportin is also capable of transporting protons, and this activity is tightly coupled to the iron transport. Remarkably, ferroportin can conduct active transport uphill against the iron gradient, with favorable charge potential providing the driving force. Targeted mutagenesis suggests that the iron translocation site is located at the pore region of human ferroportin. Together, our studies enhance the mechanistic understanding by which human ferroportin transports iron and suggest that a combination of electrochemical gradients regulates iron export.

Introduction

Ferroportin is the only iron exporter known in vertebrates.[1] At the systemic level, ferroportin exports iron into the blood plasma from most cells involved in iron metabolism,[2] including dietary iron absorbed by duodenal enterocytes,[3] stored iron released from hepatocytes,[4] and the majority of body iron that is recycled by macrophages through erythropoiesis. During pregnancy, ferroportin releases maternal iron from placenta syncytiotrophoblasts into the fetal circulation.[5] In addition to handling systemic iron flow, ferroportin maintains local iron balance in heart and other tissues.[6,7] Ferroportin has been proposed to act as a "safety valve" that relieves cardiomyocytes[8] from iron-overload conditions such as those caused by thalassemia treatment.[9-12] An important regulator of ferroportin is hepcidin,[13-15] a peptide hormone triggering the internalization and subsequent degradation of the iron exporter. This regulation represents the most important control point of systemic iron homeostasis.[2,8]

Despite the physiological importance of ferroportin, the molecular mechanism of iron export remains unclear. Ferroportin belongs to the major facilitator superfamily (MFS) of membrane transporters, most of which use a cotransport mechanism, with proton being the typical coupling ion.[16-19] The coupling enables the proton cotransporters to overcome an unfavorable substrate gradient that can occur under certain physiological conditions. The cotransport activity of ferroportin, however, is not obvious from previous studies conducted in *Xenopus* oocytes,[20,21] of which the intracellular pH cannot be controlled. In addition, it is difficult to analyze metal efflux from cells[20] because metal ions injected into the cells can be sequestered by small chelator molecules or chaperone proteins. The cellular studies[20,21] show that ferroportin can transport Fe^{2+}, Co^{2+}, and Zn^{2+} but disagree on whether ferroportin can transport Cd^{2+} and Mn^{2+}.

To resolve these difficulties, the current study determined the transport activity of purified human ferroportin in liposomes. Purified ferroportin actively transports Fe^{2+} as in cells. Other divalent metal ions, Co^{2+}, Ni^{2+}, and Mn^{2+}, are transported with decreasing affinities. Ferroportin can transport protons, and this activity requires the cotransport of Fe^{2+} (or Co^{2+}). Moreover, ferroportin can conduct

uphill active transport against a Fe^{2+} (or Co^{2+}) gradient. Mutagenesis analyses suggest that the iron translocation site is at the pore region of ferroportin. Elucidation of the transport mechanism of human ferroportin has implications for the control of iron export under various physiological settings.

Methods

Cloning and protein purification

The coding sequence of human ferroportin was amplified with polymerase chain reaction from an untagged clone (OriGene SC127301) and subcloned into a modified pPICZ-B expression vector (supplemental Figure 1A). A PreScission protease cleavage site, enhanced green fluorescent protein sequence, and 10× histidine tag were added to the C-terminal of ferroportin. Ferroportin mutants were generated by site-directed mutagenesis with the use of QuikChange. The nucleotide sequences of all the constructs were verified by DNA sequencing.

Wild-type and mutant ferroportin constructs were linearized and transformed into *Pichia pastoris*. Zeocin-resistant colonies with the highest expression level were inoculated to BMG media (1% glycerol, 0.34% yeast nitrogen base, 1% ammonium sulfate, 0.4 μg/mL biotin, and 100 mM potassium phosphate, pH 6.0) and grown at 30°C for 20 hours. After an exchange to the media without glycerol, protein expression was induced with 0.7% methanol for 2 days at 25°C. The cells were harvested by centrifugation and flash-frozen in liquid nitrogen.

For protein purification, 20 g frozen *Pichia* cells were applied to a ball mill (Retsch) to break the cell wall. The cell membrane was subsequently solubilized in a buffer containing 2% *n*-dodecyl β-D-maltoside (DDM), 300 mM NaCl, 100 mM Tris-HCl, pH 8.0, 10 μg/mL DNase I, and protease inhibitors. After centrifugation, the supernatant was incubated with Ni-NTA agarose, and the resin was subsequently washed in a buffer containing 20 mM imidazole, 50 mM Tris-HCl, pH 8.0, 150 mM NaCl, and 0.2% DDM. PreScission protease was added to remove the enhanced green fluorescent protein and 10× histidine tag from ferroportin. After the in-resin digestion, the protein was collected and concentrated for the subsequent purification by size-exclusion chromatography (Superdex 200). The peak fractions showing the highest UV absorbance (supplemental Figure 1A) were pooled and concentrated to 20 mg/mL, and the fresh protein was immediately used for liposome reconstitution.

Reconstitution of ferroportin into liposomes

The lipid mixture of 1-palmitoyl-2-oleoyl-sn-glycero-3-phosphoethanolamine and 1-palmitoyl-2-oleoyl-sn-glycero-3-phospho-(1'-rac-glycerol) at a 3:1 ratio (wt/wt) was resuspended in the reconstitution buffers used in different assays. The buffers contained 0.6% sodium cholate, and the final concentration of total lipids was 10 mg/mL. The lipid suspension was sonicated and mixed with purified ferroportin at 1:40 protein-to-lipid ratio (wt/wt). Biobeads were added to remove the DDM detergent and to promote the liposomal reconstitution of ferroportin. After 2 hours, the protein concentration of the supernatant containing proteoliposomes was measured with a bicinchoninic acid assay and adjusted to the same protein concentration for wild-type and mutant ferroportins. The proteoliposomes were stored on ice before the transport assays.

Transport assay of divalent metal ions

The reconstitution buffer used for the metal transport assay contained 150 mM NaCl and 25 mM of different pH buffers, which are MES-NaOH pH 6.0, MES-NaOH pH 6.5, HEPES-NaOH pH 7.0, HEPES-NaOH pH 7.5, and Tris-HCl pH 8.0. These pH buffers and the buffers containing 5 mM $CaCl_2$ were used during the lipid resuspension and ferroportin reconstitution. After the reconstitution, the proteoliposomes were mixed 1:1 (vol/vol) with the reconstitution buffers containing 500 μM calcein. Calcein was enclosed into the proteoliposomes through 3 freeze-thaw cycles and sonication. The proteoliposomes were subsequently passed through a G50 desalting column to remove free calcein and to exchange the buffers outside of the liposomes.

The metal transport assay was performed in 96-well plates with a Synergy 2 plate reader (BioTek), and the calcein fluorescence was detected with the excitation wavelength at 494 nm and emission at 516 nm. After 5 minutes equilibration, 10 μM $FeCl_2$, 100 μM $CoCl_2$, 100 μM $MnCl_2$, or 100 μM $NiCl_2$ was added. For the competition assay, 100 μM of $ZnCl_2$, $CdCl_2$, $CaCl_2$, or $MgCl_2$ was added together with 10 μM $FeCl_2$. The metal transport through ferroportin was monitored for another 20 minutes. At 25 minutes, 1 μM calcimycin was added to allow metal influx through this ionophore. The intensity of the calcein fluorescence at 25 minutes was expressed as a percentage of the fluorescence before the metal ions were added (between 0 and 5 minutes), and this was used as a measure of transport activity.

Proton transport assay

The proteoliposomes were enclosed with a reconstitution buffer containing 150 mM KCl and 25 mM HEPES-KOH pH 7.5. Subsequently, the proteoliposomes were flowed through a G50 column prewashed with 150 mM NaCl and 25 mM HEPES pH 7.5. For the analysis of proton uptake, the same buffer with 1 μM 9-amino-6-chloro-2-methoxyacridine (ACMA) was added at the outside of the liposome; ACMA can diffuse freely into the liposomes but cannot diffuse out once it is proton bound.[22] The ACMA fluorescence was detected with an excitation wavelength at 410 nm and emission at 490 nm. After 5 minutes of equilibration, 10 μM $FeCl_2$ (or 20 μM $CoCl_2$) and 20 nM valinomycin were added to generate an electrochemical gradient. The proton transport through ferroportin was monitored for another 20 minutes. At 25 minutes, 1 μM carbonyl cyanide *m*-chlorophenyl hydrazone (CCCP) was added to allow proton influx through this proton channel. The intensity of the ACMA fluorescence at 25 minutes was expressed as a percentage of the fluorescence before the metal ions were added (between 0 and 5 minutes), and this was used as a measure of proton transport activity.

Assay of active transport against the Fe^{2+}/Co^{2+} concentration gradient

For the analysis of active transport, the reconstitution buffer enclosed in proteoliposomes was 25 mM HEPES pH 7.5, 150 mM KCl, 100 μM $FeCl_2$ (supplemented with 100 μM sodium ascorbate to prevent oxidation), or 100 μM $CoCl_2$. The proteoliposomes were quickly flowed through a G50 spin column and immediately used for the transport assay. To measure proton transport, a buffer containing 25 mM HEPES pH 7.5, 150 mM NaCl, and 1 μM ACMA was added from the outside of the liposome.
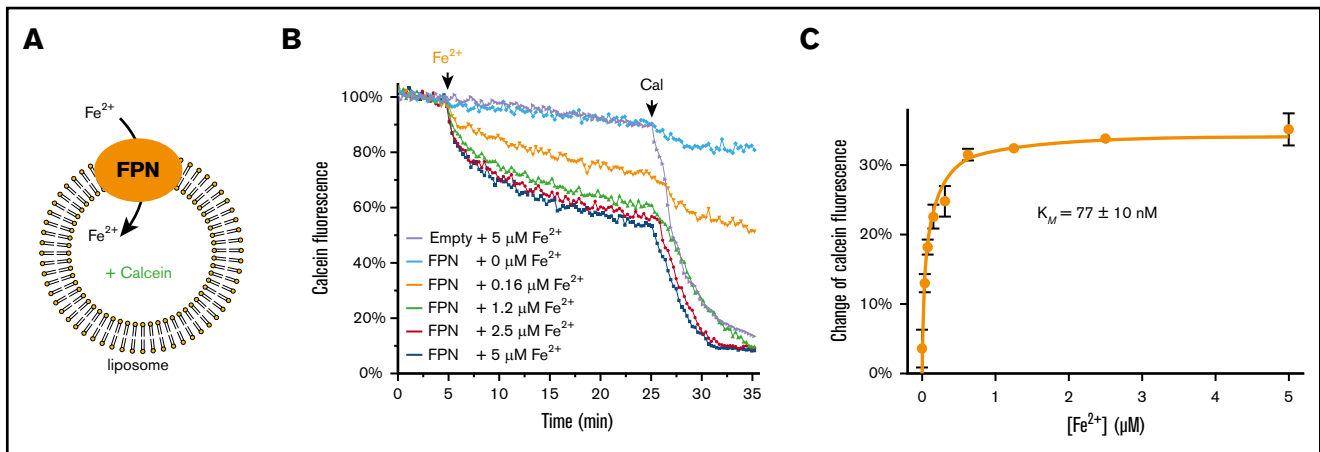
Figure 1. Purified human ferroportin (FPN) actively transports iron into liposomes. (A) Fluorescence-based assay of Fe^{2+} transport by FPN. The chemical gradient of Fe^{2+} drives the Fe^{2+} transport by FPN into the liposome. The Fe^{2+} influx is detected by the quenching of calcein fluorescence enclosed in the liposome. (B) Time-resolved FPN transport of Fe^{2+}. The representative curves show the fluorescence quenching at different Fe^{2+} concentrations. Addition of Fe^{2+} and calcimycin (Cal) are indicated above the curves. The FPN-mediated Fe^{2+} transport is between 5 and 25 minutes and is saturated at high Fe^{2+} concentrations. Empty liposomes and FPN-containing liposomes with 0 μM Fe^{2+} are used as controls. (C) Michaelis-Menten curve of Fe^{2+} transport. The error bar of each data point is from duplicated experiments. Error of the apparent K_M is calculated from the curve fitting of the duplicates by GraphPad Prism.

After 5 minutes equilibration, 1 μM $FeCl_2$ (with 1 μM sodium ascorbate) or 1 μM $CoCl_2$ and 20 nM valinomycin were added. The proton transport through ferroportin was monitored for another 20 minutes. At 25 minutes, 1 μM CCCP was added to allow proton influx through this proton channel.

Results

Purified human ferroportin in a liposomal system transports iron efficiently

To conduct the transport assay in proteoliposomes, we expressed human ferroportin in *P pastoris* and purified the protein (supplemental Figure 1). During the purification, the wild-type protein (and mutant proteins used in later experiments) showed one major peak on size-exclusion chromatography. The wild-type ferroportin was reconstituted into liposomes, which was subsequently enclosed with calcein, a fluorophore that specifically binds divalent ions (Figure 1A). Fe^{2+} and other divalent metal ions (M^{2+}) were provided from the outside of the liposomes to generate an influx gradient, and metal ions transported into the liposomes were detected by the quenching of calcein fluorescence.[23,24]

The reconstituted ferroportin shows a large activity of Fe^{2+} transport (Figure 1B). At high Fe^{2+} concentrations (1.2-5 μM), the calcein fluorescence is quenched to ~50% to 60%. As a control, calcimycin, a divalent cation ionophore, was added later to allow untransported Fe^{2+} to cross liposome membranes. In the presence of calcimycin, the fluorescence is lowered by another ~40%. In contrast, the empty liposome without ferroportin incorporated shows little decrease of fluorescence (~10%), whereas adding calcimycin lowers the fluorescence by another ~80%. Taken together, ferroportin can transport a large fraction of iron provided to the liposomal system.

To further validate the liposomal assay of ferroportin activity, we showed that the Fe^{2+} transport mediated by ferroportin follows Michaelis-Menten kinetics (Figure 1C). The Fe^{2+} influx is saturated at moderate to high Fe^{2+} concentrations. If Fe^{2+} had entered the

proteoliposomes by significant leakage, the apparent influx would have increased proportionally with the Fe^{2+} gradient. Instead, this saturability is due to the limit imposed by ferroportin transport, and the Fe^{2+} influx is primarily through ferroportin. The apparent Michaelis constant (K_M) of Fe^{2+} is 0.077 μM, close to the apparent affinity constant (≤0.1 μM) estimated from a cellular assay[20]; this consistency indicates that the reconstituted ferroportin has a similar activity as in the cellular environment and that the liposomal assay can mimic physiological conditions.

Human ferroportin preferentially transports iron over other divalent metal ions

We tested the transport of other divalent metal ions by ferroportin (Figure 2A-B) to compare with the cellular studies.[20,21] The apparent K_M for Co^{2+} transport is 5.2 μM, consistent with the apparent affinity constant of ≤5 μM from the cellular assay.[20] Ferroportin can also transport Ni^{2+} ($K_M = 12.7$ μM) in vitro; this Ni^{2+} transport activity has not been directly shown before.[21] Ferroportin is a poor transporter of Mn^{2+}, with a K_M of 40 μM and a lower V_{max} (maximum rate of transport) compared with other metals. This apparent K_M of Mn^{2+} is lower than that observed in cellular assays (~740 μM), probably because most Mn^{2+} is sequestered in cells and free Mn^{2+} is at a low concentration. The K_M of Mn^{2+} is nevertheless high, supporting the assertion that Mn^{2+} is unlikely a physiological substrate of ferroportin. It remains possible, however, that ferroportin may slowly detoxify Mn^{2+} given a prolonged period of time. Our in vitro assay cannot analyze the activity of Cu^{2+} because it causes a precipitation of the proteoliposome. In addition, Ca^{2+}, Mg^{2+}, Cd^{2+}, and Zn^{2+} do not quench calcein fluorescence. To overcome this problem, we analyzed the competition[23] of these ions against Fe^{2+} transport (Figure 2C). Ca^{2+} and Mg^{2+} at 100 μM do not affect Fe^{2+} transport. In contrast, 100 μM Cd^{2+} and Zn^{2+} can inhibit the transport of Fe^{2+} (10 μM), suggesting that ferroportin may be able to transport Cd^{2+} and Zn^{2+}. Taken together, it is clear that ferroportin can transport several divalent transition-metal ions in addition to Fe^{2+}. Given that
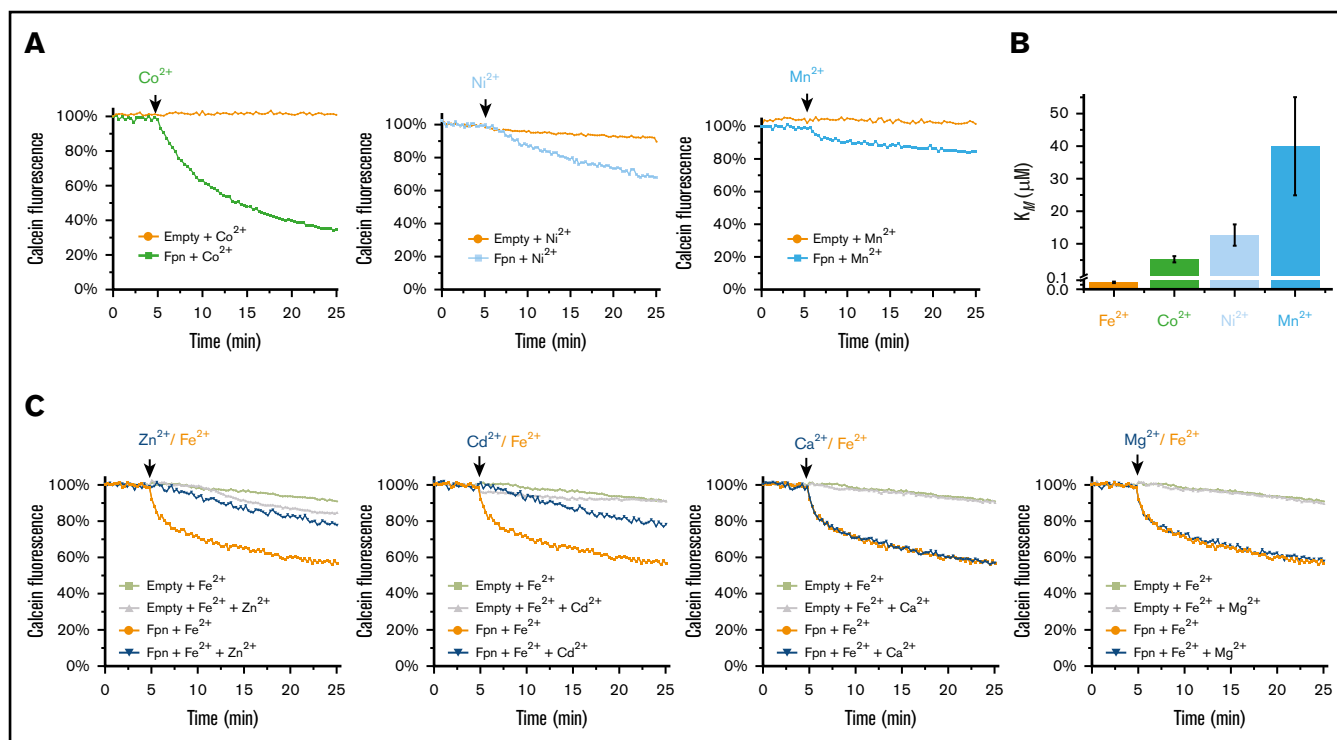
Figure 2. Human ferroportin preferably transports Fe^{2+} over other divalent metal ions. (A) Transport activity of Co^{2+}, Ni^{2+}, and Mn^{2+} using the calcein-based assay (as in Figure 1). Addition of these divalent metal ions is indicated above the curves. All metal ions are provided at the concentration of 100 μM. (B) Comparison of the apparent K_M of ferroportin-mediated transport of different metal ions, with the y-axis break at 0.1 μM. (C) Competition of other divalent ions (Zn^{2+}, Cd^{2+}, Ca^{2+}, and Mg^{2+}) against Fe^{2+} transport. Fe^{2+} and the competing metal ions are provided at the concentrations of 10 μM and 100 μM, respectively.

Co^{2+} is more resistant to oxidation, we included Co^{2+} in subsequent experiments to compare with Fe^{2+} transport. The apparent K_M of Fe^{2+} is much lower than that of Co^{2+}, Ni^{2+}, and Mn^{2+}, indicating that ferroportin preferentially exports Fe^{2+} over other divalent metal ions.

Proton gradients facilitate the iron transport by ferroportin at the same direction

With the liposomal transport assay established, we investigated whether the iron transport of human ferroportin can be altered by proton gradients (Figure 3A). We first tested the pH profile of iron transport activity in the absence of a proton gradient. With the same pH maintained at the inside and outside of proteoliposomes, we found that ferroportin is maximally active at pH 7.5 but loses most of its Fe^{2+} or Co^{2+} transport activity at pH 6 and pH 8 (Figure 3B-C), consistent with previous cellular assays.[20] To generate proton gradients, we kept pH 7 at one side of the liposomes and varied the pH at the other side. With the pH gradients, the most notable change in the pH profiles is that the maximum activity of Fe^{2+} or Co^{2+} transport is now observed at pH 8 inside, when pH 7 is provided at the outside (pH $8_{in}/7_{out}$) (Figure 3B-C). When pH 7 is provided at the inside, a notable difference is that $7_{in}/6_{out}$ shows a higher activity than pH $6_{in}/6_{out}$ and pH $6_{in}/7_{out}$. The complicated changes in the activity levels reflect combined effects from the proton gradients, the intrinsic pH profile of ferroportin, and the unidirectional Fe^{2+} or Co^{2+} gradient being applied to the system. When larger proton gradients were applied (Figure 3D-E), the highest Fe^{2+} or Co^{2+} transport activity is observed with pH $8_{in}/6_{out}$.

Taken together, the inward transport of Fe^{2+} (or Co^{2+}) by ferroportin can be stimulated by the inward proton gradient across the membrane.

Apart from the proton gradient, a recent report found that extracellular Ca^{2+} stimulates ferroportin activity in cells.[25] With the purified system, here we show that Ca^{2+} inside the liposome enhances the Fe^{2+} transport activity of ferroportin (Figure 3F), consistent with the cellular assays. In contrast, Ca^{2+} at the outside has no stimulatory effect. Thus, Ca^{2+} needs to be present at the side toward which ferroportin transports Fe^{2+}; this directionality is conceptually the same as observed with cellular assays, in which iron export requires extracellular Ca^{2+}. Because Ca^{2+} and proton gradient both enhance Fe^{2+} transport, we investigated the relationship between these 2 stimulators. We found that the transport activity increases by approximately fourfold with pH $8_{in}/6_{out}$, and increases by sixfold with 5 mM Ca^{2+} at pH $8_{in}/8_{out}$. When 5 mM Ca^{2+} and pH $8_{in}/6_{out}$ are both applied, the activity increases cumulatively to 10-fold. This observation suggests that the extracellular Ca^{2+} and proton gradient may act together to enhance (or regulate) ferroportin activity under physiological conditions.

Ferroportin is a proton symporter

To detect whether ferroportin can transport proton, we used an ACMA fluorophore to follow the change of proton concentration in proteoliposomes[22] (Figure 4A). To allow sufficient pH change detectable by the quenching of ACMA, we need to neutralize the positive charges that are built up after Fe^{2+} (and H^+) influx and

Figure 3. Proton gradients facilitate Fe^{2+} and Co^{2+} transport in the same direction. (A) Assay of the Fe^{2+} transport activity (same as in Figure 1) with the variations of pH inside and outside the liposome. (B) Comparison of the pH profiles of Fe^{2+} transport with and without proton gradients. The same pHs inside and outside the liposomes (green curve) show the pH dependence of ferroportin (FPN) activity without a proton gradient. The proton gradients across the membrane are generated by keeping pH 7 at inside (blue curve) or outside (red curve) the liposomes and varying the pHs at the other side. Fe^{2+} is provided at 10 μM concentration. (C) Comparison of the pH profiles of Co^{2+} transport with and without proton gradients. Co^{2+} is provided at 100 μM concentration. (D-E) Relative Fe^{2+} and Co^{2+} transport activities with proton gradients between pH 6 and pH 8. All error bars are standard deviations from 3 repeats. (F) Fe^{2+} transport activities with 5 mM Ca^{2+} inside and/or outside the liposomes. (G) Fe^{2+} transport activities with 5 mM Ca^{2+} inside and with proton gradients between pH 6 and pH 8.
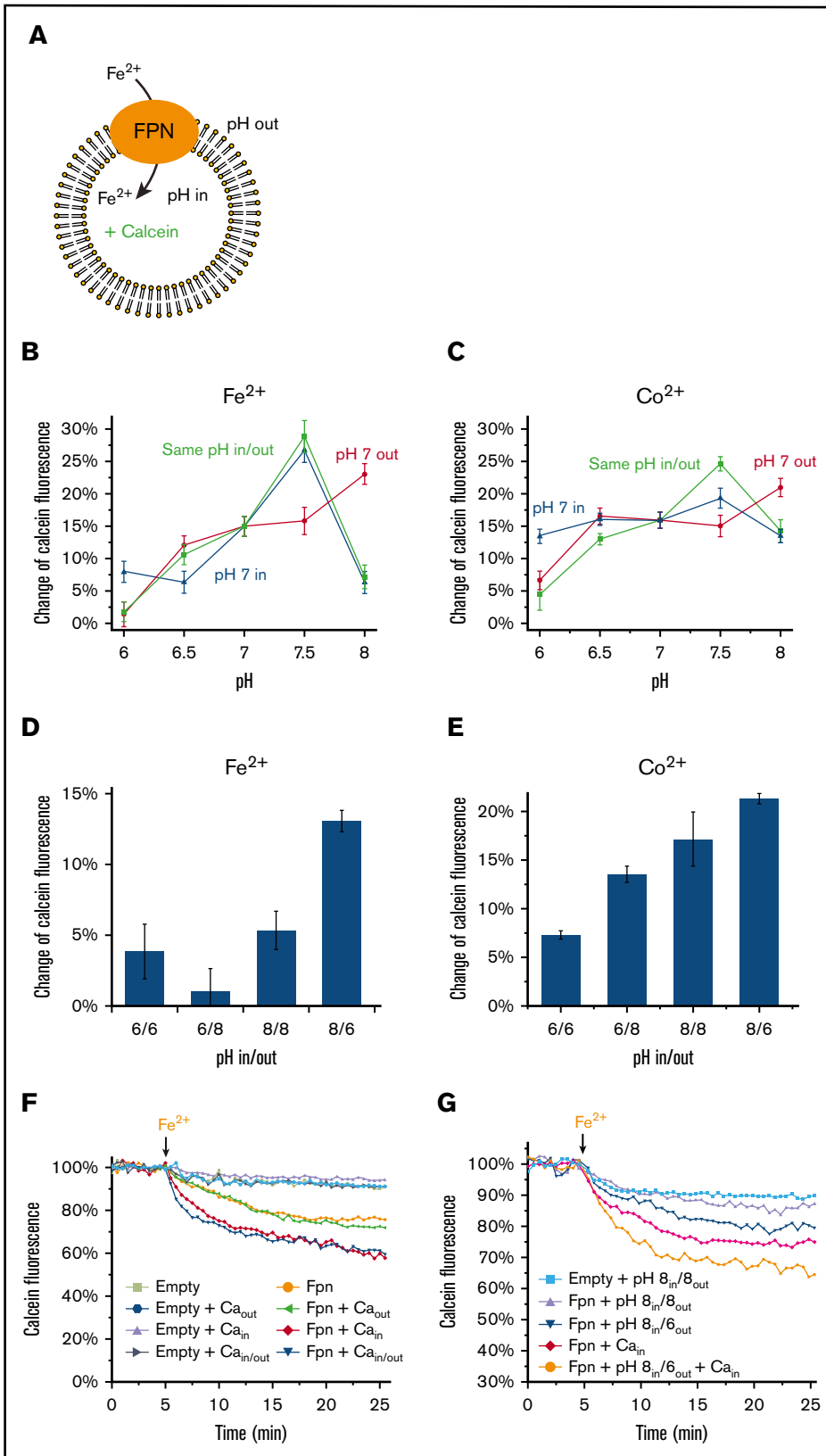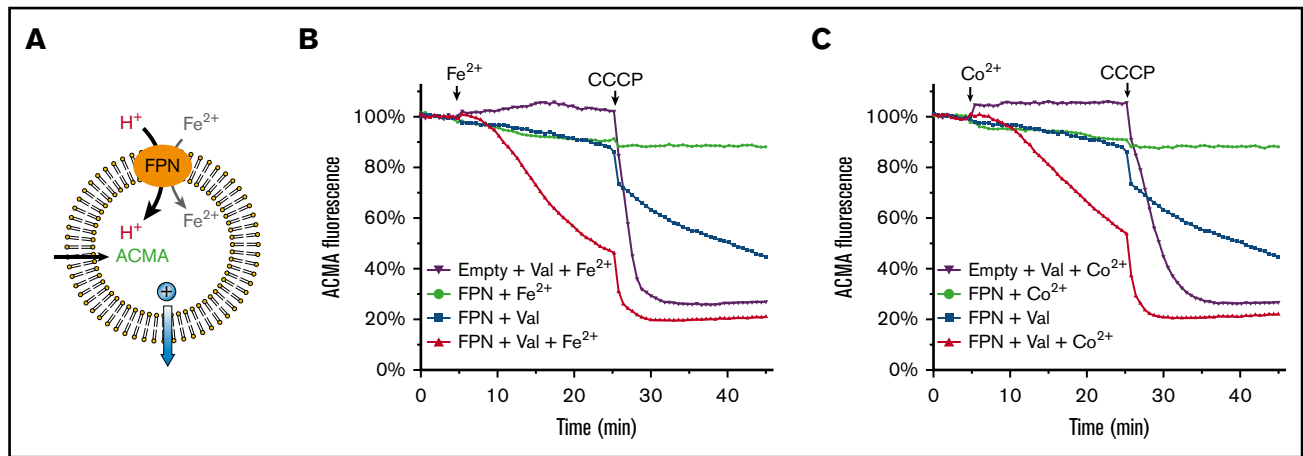
Figure 4. Human ferroportin (FPN) transports proton along the iron gradient. (A) Assay of proton transport based on the quenching of ACMA fluorescence. ACMA is provided from the outside to diffuse into the liposome[22] (black arrow). After proton is bound, ACMA cannot diffuse out. To promote proton transport by FPN, 10 μM Fe^{2+} is provided at the outside to generate an influx gradient. The positive charge (blue sphere) introduced by Fe^{2+} and H^+ influx is compensated for by K^+ outflow through valinomycin (blue arrow). (B) Proton transport by FPN requires a Fe^{2+} gradient. Addition of Fe^{2+} at 5 minutes and CCCP at 25 minutes are indicated above the curves, and valinomycin (Val) is added at 0 minutes. (C) Proton transport by FPN in the presence of a Co^{2+} gradient. To generate an influx gradient, 100 μM Co^{2+} is provided from the outside of the liposome. Other experimental setups are the same as in panel B.

that prevent further influx. We therefore loaded liposome with KCl inside and an equal concentration of NaCl outside, and added valinomycin, a K^+ ionophore, to allow selective outflow of K^+, thereby generating counteractive negative charges inside the liposome.

In the presence of ferroportin, significant proton influx is observed when the Fe^{2+} or Co^{2+} gradient and the negative charge potential are applied together (Figure 4B-C). In contrast, the charge potential alone does not promote much proton inflow. The Fe^{2+}/Co^{2+} gradient alone only promotes low proton inflow due to the accumulation of positive charges. As a control, CCCP, a proton channel, was added later to allow further proton influx, and the relative levels of fluorescence quenching confirm that the proton influx mediated by ferroportin is significant. Taken together, ferroportin is capable of transporting protons, and the proton transport requires the presence of Fe^{2+}/Co^{2+}. The downhill Fe^{2+}/Co^{2+} gradient used here should also promote the Fe^{2+}/Co^{2+} transport (Figure 1). Because the Fe^{2+} and H^+ are cotransported in the same direction, ferroportin is an Fe^{2+}/H^+ symporter.

Ferroportin mediates secondary active transport

Proton symporters should support secondary active transport.[26-28] Therefore, in principle, a favorable electrochemical potential will drive ferroportin to move Fe^{2+} or Co^{2+} uphill against its concentration gradient. To demonstrate this active transport, we set the Fe^{2+}/Co^{2+} concentrations at 1 μM outside the proteoliposomes and 100 μM inside (Figure 5A). The uphill influx was driven by a negative-inside charge potential, generated from selective K^+ efflux as explained earlier. Direct analysis of the Fe^{2+}/Co^{2+} transport activity is, however, infeasible because the calcein fluorophore binds the metal ions and lowers their concentration inside the liposome to an unknown level. Thus, we analyzed proton transport instead.[23] A large proton influx, which was driven by the charge potential, was observed against the uphill Fe^{2+}/Co^{2+} gradient (Figure 5B-C). Remarkably, if

Fe^{2+}/Co^{2+} was not provided from the outside, the proton transport did not occur, indicating that the proton transport is tightly coupled to the Fe^{2+}/Co^{2+} transport. Because of this coupling, the proton transport indicates the uphill transport of Fe^{2+}/Co^{2+} against their chemical gradients. Taken together, these data show that the symport of Fe^{2+}/Co^{2+} and proton can be driven uphill against the chemical gradient of Fe^{2+}/Co^{2+}.

Mutations disrupting the iron and proton transport activities of ferroportin

To understand the structural basis of iron export, we built homology models[29] of human ferroportin (Figure 6A) based on the crystal structures of a bacterial homolog.[24] The bacterial structures were determined at the inward- and outward-facing conformations, which allow alternating access during the substrate transport, a mechanism believed to be used by all MFS transporters.[16] In this bacterial homolog, the iron-binding site is located at the N-half of the protein (N-lobe) and buried in the transmembrane helices. The iron is coordinated by 4 residues (T20, D24, N196, and S199) in the crystal structures of the bacterial homolog; in human ferroportin, the corresponding residues constituting this putative iron-bind site are S35, D39, N212, and S215, respectively. Biochemical analyses of the bacterial homolog show that the D24A mutant has drastically reduced transport activity.[24] In addition, the iron-binding affinity is lowered by several folds with D24A, N196A, and D24A/N196A mutations.

We mutated D39 and N212 in human ferroportin to determine whether it shares the same iron-binding site as the bacterial homolog. Surprisingly, we found that mutations of D39A, N212A, D39A/N212A, and H32A, a nearby residue (Figure 6A), all retain a similar activity of iron transport as the wild-type human ferroportin (supplemental Figure 2A). Moreover, the apparent K_M values of D39A, N212A, D39A/N212A, and H32A are similar or even better than that of the wild-type ferroportin (supplemental Figure 2B). Because mutating the iron-binding site is expected to change the
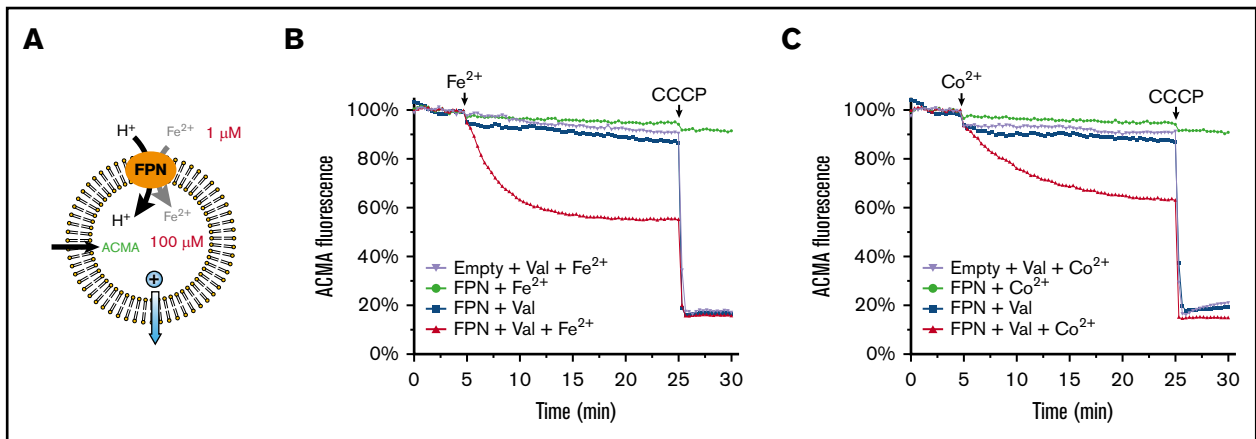
Figure 5. Human ferroportin (FPN) supports uphill active transport. (A) Assay of proton transport with an uphill Fe^{2+} gradient. The gradient is generated by enclosing 100 μM Fe^{2+} inside the liposome and providing 1 μM Fe^{2+} from the outside. The influx of Fe^{2+} and H^+ is promoted by a charge gradient that is generated from the K^+ outflow through valinomycin (Val; blue arrow). The assay of proton transport by the quenching of ACMA fluorescence is the same in Figure 4. (B) FPN transports protons against an uphill Fe^{2+} gradient. Addition of Fe^{2+} and CCCP are indicated above the curves. (C) FPN transports protons against an uphill Co^{2+} gradient, with 100 μM Co^{2+} enclosed inside the liposome and 1 μM Co^{2+} provided from the outside.

iron-transport activities and the apparent K_M, these ineffective mutations suggest that the iron-binding site of human ferroportin is different from that of the bacterial homolog.

The N-lobe location of the iron-binding site in the bacterial homolog is known to be unusual (Figure 6A) because all other MFS transporters with known structures bind substrates at the interface between the N- and C-lobes.[16] The homology models of human ferroportin show several acidic and histidine residues around this interface region, including H32, D39, D181, E219, D254, D325, D473, E486, D504, and H507; these residues are capable of binding iron or protonate under a physiological pH. We therefore mutated all of these candidate residues to identify those involved in proton and iron transport. Among the 12 mutants tested, only D181N exhibits low Fe^{2+} or Co^{2+} transport activity, suggesting that D181 is involved in the iron binding (Figure 6B-C). In addition, D181N has a low proton transport activity compared with the wild-type ferroportin (Figure 6D-E). The homology models show that D181 can be alternatively accessed at the inward- and outward-facing conformations, supporting that D181 constitutes part of the iron-translocation pore.

Unlike D181N, several other mutants can actively transport Fe^{2+} /Co^{2+} but exhibit low activities of transporting proton, indicating that these 2 activities can be decoupled (Figure 6D-E). The E219A and E486A mutants both can decouple the proton-iron symport. E219Q, however, is active for both Fe^{2+}/Co^{2+} and proton transport, whereas E486Q mutant decouples the symport; these mutations were tested because the glutamine side chain cannot be protonated. D254N drastically lowers the proton transport activity, whereas D39N, D325N, and D473N exhibit ~50% to 60% of activity compared with the wild-type ferroportin. In contrast, H32A, D504N, and H507A remain largely active for iron and proton transport. These residues are unlikely to be involved in the transport process. Taken together, decoupling of iron and proton transport activities is probably because the mutations disrupt the protonation or deprotonation process during the ferroportin-mediated transport.

Discussion

In this study, we established a liposomal assay to analyze the transport activities of purified human ferroportin. This proteoliposome system enables the precise characterization of transport activities of human ferroportin and avoids limitations of cell-based assays (Figure 1). For example, it is difficult to measure proton transport or to control the concentration of free iron in cells. Compared with iron export from cells, the iron import into the proteoliposomes is in a reversed direction but is conceptually equivalent. Ferroportin can transport iron into liposomes with an apparent K_M at the submicromolar range, consistent with the cell-based assays. This low K_M allows ferroportin to efficiently transport iron even at low cellular concentrations.

Ferroportin shows considerable activity of transporting several other transition metal ions, suggesting that ferroportin may also export these metals from various cells. The exporter activity of ferroportin is unusual among the numerous metal transporters found in cells, most of which are importers of metal ions.[30] Thus, this unusual exporter may be used in vivo for protection against the cytotoxicity caused by overload of transition metal ions. Compared with Fe^{2+} transport, however, ferroportin exhibits a much larger K_M of transporting other transition metals (Figure 2B). Thus, it is possible that ferroportin does not affect the normal metabolism of these metals but acts as a safety valve when these metal ions exceed certain cellular levels. Furthermore, overloaded iron and other transition metals are known to induce ferroportin expression in various cells, such as macrophages.[31-36] This regulatory mechanism may serve as another trigger for ferroportin to export these transition metals and detoxify cells.

Ferroportin exhibits tightly coupled activities of proton and iron transport at the same direction (Figure 4B-C). The mechanism of proton symport is most well studied in LacY, a canonical MFS transporter.[26] Protonation of LacY is required for substrate binding, which induces the transition between the inward- and outward-facing conformations. This structural transition allows substrate release, which is associated with side chain rearrangements that involve deprotonation. If ferroportin shares a similar mechanism as
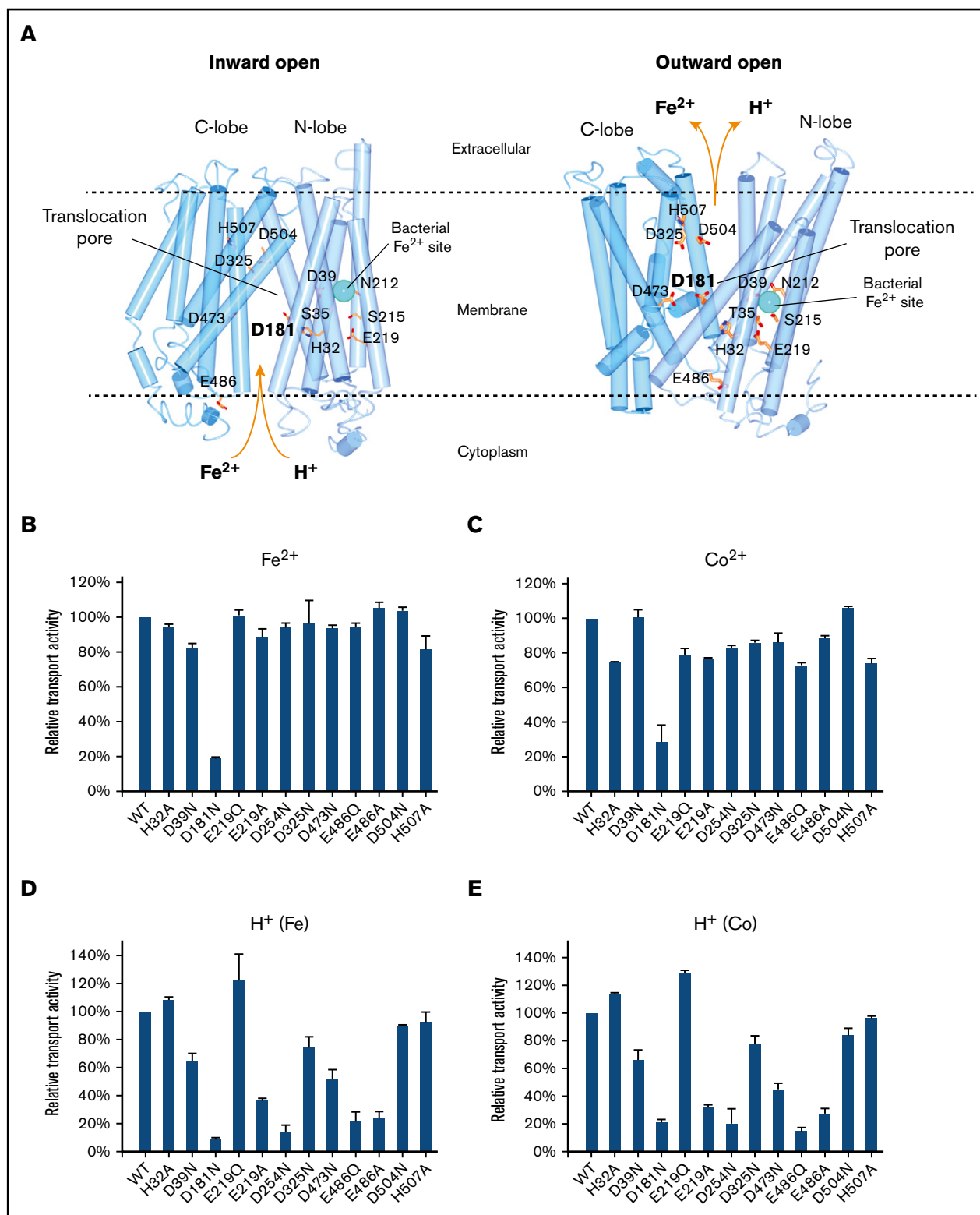
13 OCTOBER 2020 · VOLUME 4, NUMBER 19   🩸 **blood** advances

Figure 6. Iron and proton transport activities of ferroportin mutants. (A) Homology model of human ferroportin in inward-open (left) and outward-open (right) conformations. The models are generated by I-TASSER[45] using the PDB code 5AYN and 5AYO. The iron-binding site in the bacterial homolog is shown in cyan sphere. (B-C) Relative Fe^{2+} and Co^{2+} transport activities of mutants. Experimental setups are the same as in Figure 1. (D-E) Relative proton transport activities of the mutants under a Fe^{2+} and Co^{2+} gradient. Experimental setups are the same as in Figure 4.

LacY, the tight coupling between proton and iron transport can also be explained. By analogy, iron binding at the inward-facing conformation is required to induce the structural transition to the outward-facing conformation to release iron. In the absence of the iron binding and release, the proton transport, which involves protonation and deprotonation at the alterative conformations, becomes insignificant (Figure 5B-C).

Ferroportin uses multiple mechanisms to enhance its transporter activity. Inspired by a previous report,[25] here we found that the presence of Ca^{2+} increases ferroportin activity in the purified liposomal system (Figure 3F). Because Ca^{2+} and proton gradient enhance the ferroportin activity cumulatively (Figure 3G), they seem to use different mechanisms, presumably through modulating the protein conformation in different ways; if a similar mechanism were used, Ca^{2+} and proton gradient should have overcome the need of each other for enhancing the activity. Moreover, iron export into the blood plasma is facilitated by ferroxidases[8] such as ceruloplasmin and hephaestin, which oxidize Fe^{2+} to Fe^{3+}.

Among the mutants of 11 acidic or histidine residues we tested, D181N is the only one inactive for both iron and proton transport (Figure 6B-E). The homology models of human ferroportin show that D181 is located at the interface between the N- and C-lobes, a location consistent with that of the translocation pore (Figure 6A). If the iron binding is disrupted by D181N, the structural transition cannot be induced to allow proton transport, consistent with the loss of both activities. Clinically, a D181V mutation leads to ferroportin disease, suggesting the importance of this residue in the function of iron export.[37] Moreover, the region around D181 on TM5 is a hotspot of ferroportin disease mutations, including N174I, R178Q, I180T, Q182H, and N185D/T.[38-40] The cluster of these mutations also suggests that the translocation site is located around D181. Taken together, the iron translocation by human ferroportin probably involves D181, and this translocation site is at the pore region, similar to other MFS transporters.

This pore location of iron binding and translocation site is different from that reported in the bacterial homolog.[24] Due to the considerable sequence similarity, the overall structures of human ferroportin should be largely similar to the crystal structures of the bacterial homolog, which has revealed an unusual iron-binding site at the N-lobe of the bacterial protein. However, human ferroportin mutants at this site can transport iron with similar V_{max} and K_M as the wild-type protein, unlike the corresponding mutants of the bacterial homolog. Thus, our data indicate key differences between the human ferroportin and its bacterial homolog, the latter of which is also not a proton symporter.

Several mutations can decouple the proton transport from iron transport. For instance, the E486Q mutant mimics the protonated form of E486, allowing ferroportin to bind iron with high affinity and to conduct iron transport, but this mutant cannot transport proton (Figure 6B-E). The homolog model at the outward-facing conformation shows that E486 is at the C-lobe of ferroportin and forms a salt bridge with R88 at the N-lobe. At the inward-facing conformation, however, these residues are far apart, thereby allowing the protonation of E486. However, E486 is located at the intracellular surface and not exposed to the extracellular side at the outward-facing conformation (Figure 6A). Because E486 cannot be deprotonated at the outward-facing conformation, the proton transport cannot be mediated by E486 alone. Instead, this residue probably serves as the initial proton-binding site on a translocation path, whereas the actual residues mediating the proton transport remain to be identified. Similar to LacY, protonation of ferroportin may increase its affinity of iron binding; in LacY, the protonation is on a glutamate residue, which does not bind the substrate directly but donates the proton to assist substrate binding.[41] Overall, the structural mechanism of proton-symport in ferroportin remains to be answered.

Proton coupling is broadly used by MFS transporters as the energy source to conduct active transport.[16] The efficiency of iron export is determined by the iron and proton gradient. Membrane potential also contributes to the overall electrochemical gradient because ferroportin is an electrogenic symporter of Fe^{2+} and H^+. The negative charge potential inside cells is against the export of the positively charged Fe^{2+} and H^+. Theoretically, for the Fe^{2+} export to occur, the regular membrane potential of −60 mV requires a 1000-fold concentration gradient of Fe^{2+} across the plasma membrane (assuming one proton cotransports with one Fe^{2+}). To overcome this unfavorable and potentially controlling barrier of membrane potential, one plausible solution is to coordinate iron export with iron import in various cell types. In duodenal enterocytes, iron[41-43] and many other nutrients are imported through various proton symporters[8] (supplemental Figure 3A). In macrophages, iron released in the phagolysosome is also transported to cytoplasm by proton symporters, DMT1[18] and Nramp1 (supplemental Figure 3B). These protons, together with the imported iron, may generate sufficient driving force for iron export. As an exception, cardiomyocytes constantly depolarize to generate a reversed membrane potential, which may facilitate iron export and protect these cells against iron overdose[44] (supplemental Figure 3C). Examining these hypotheses under physiological or cellular conditions will shed light on the control and driving force of iron export in vivo.

Authorship

Contribution: S.L. performed the experiments; Y.Y. purified the proteins; and W.L. and S.L. designed the study, analyzed data, and wrote the manuscript.

Conflict-of-interest disclosure: The authors declare no competing financial interests.

ORCID profiles: S.L., 0000-0002-8930-4072; W.L., 0000-0002-8711-1904.

Correspondence: Weikai Li, Department of Biochemistry and Molecular Biophysics, Washington University School of Medicine, 660 S Euclid Ave, St. Louis, MO 63110; e-mail: weikai@wustl.edu.

References

1. Donovan A, Brownlie A, Zhou Y, et al. Positional cloning of zebrafish ferroportin1 identifies a conserved vertebrate iron exporter. *Nature*. 2000; 403(6771):776-781.

2. Ganz T. Systemic iron homeostasis. *Physiol Rev*. 2013;93(4):1721-1741.

3. Canonne-Hergaux F, Donovan A, Delaby C, Wang HJ, Gros P. Comparative studies of duodenal and macrophage ferroportin proteins. *Am J Physiol Gastrointest Liver Physiol*. 2006;290(1):G156-G163.

4. Ramey G, Deschemin JC, Durel B, Canonne-Hergaux F, Nicolas G, Vaulont S. Hepcidin targets ferroportin for degradation in hepatocytes. *Haematologica*. 2010;95(3):501-504.

5. Sangkhae V, Nemeth E. Placental iron transport: the mechanism and regulatory circuits. *Free Radic Biol Med*. 2019;133:254-261.

6. Lakhal-Littleton S, Wolna M, Carr CA, et al. Cardiac ferroportin regulates cellular iron homeostasis and is important for cardiac function [published correction appears in *Proc Natl Acad Sci U S A*. 2015;112(14):E1812]. *Proc Natl Acad Sci U S A*. 2015;112(10):3164-3169.

7. Lakhal-Littleton S, Wolna M, Chung YJ, et al. An essential cell-autonomous role for hepcidin in cardiac iron homeostasis. *eLife*. 2016;5:e19804.

8. Drakesmith H, Nemeth E, Ganz T.. Ironing out ferroportin. *Cell Metab*. 2015;22(5):777-787.

9. Arezes J, Nemeth E. Hepcidin and iron disorders: new biology and clinical approaches. *Int J Lab Hematol*. 2015;37(Suppl 1):92-98.

10. Murphy CJ, Oudit GY. Iron-overload cardiomyopathy: pathophysiology, diagnosis, and treatment. *J Card Fail*. 2010;16(11):888-900.

11. Kremastinos DT, Farmakis D. Iron overload cardiomyopathy in clinical practice. *Circulation*. 2011;124(20):2253-2263.

12. Das SK, Wang W, Zhabyeyev P, et al. Iron-overload injury and cardiomyopathy in acquired and genetic models is attenuated by resveratrol therapy. *Sci Rep*. 2015;5(1):18132.

13. Nemeth E, Tuttle MS, Powelson J, et al. Hepcidin regulates cellular iron efflux by binding to ferroportin and inducing its internalization. *Science*. 2004; 306(5704):2090-2093.

14. Qiao B, Sugianto P, Fung E, et al. Hepcidin-induced endocytosis of ferroportin is dependent on ferroportin ubiquitination. *Cell Metab*. 2012;15(6): 918-924.

15. Ross SL, Tran L, Winters A, et al. Molecular mechanism of hepcidin-mediated ferroportin internalization requires ferroportin lysines, not tyrosines or JAK-STAT. *Cell Metab*. 2012;15(6):905-917.

16. Quistgaard EM, Löw C, Guettou F, Nordlund P. Understanding transport by the major facilitator superfamily (MFS): structures pave the way. *Nat Rev Mol Cell Biol*. 2016;17(2):123-132.

17. Law CJ, Maloney PC, Wang DN. Ins and outs of major facilitator superfamily antiporters. *Annu Rev Microbiol*. 2008;62(1):289-305.

18. Pujol-Giménez J, Hediger MA, Gyimesi G. A novel proton transfer mechanism in the SLC11 family of divalent metal ion transporters. *Sci Rep*. 2017;7(1): 6194.

19. Shi Y. Common folds and transport mechanisms of secondary active transporters. *Annu Rev Biophys*. 2013;42(1):51-72.

20. Mitchell CJ, Shawki A, Ganz T, Nemeth E, Mackenzie B. Functional properties of human ferroportin, a cellular iron exporter reactive also with cobalt and zinc. *Am J Physiol Cell Physiol*. 2014;306(5):C450-C459.

21. Madejczyk MS, Ballatori N. The iron transporter ferroportin can also function as a manganese exporter. *Biochim Biophys Acta*. 2012;1818(3):651-657.

22. Feng L, Campbell EB, MacKinnon R. Molecular mechanism of proton transport in CLC Cl-/H+ exchange transporters. *Proc Natl Acad Sci U S A*. 2012; 109(29):11699-11704.

23. Ehrnstorfer IA, Geertsma ER, Pardon E, Steyaert J, Dutzler R. Crystal structure of a SLC11 (NRAMP) transporter reveals the basis for transition-metal ion transport. *Nat Struct Mol Biol*. 2014;21(11):990-996.

24. Taniguchi R, Kato HE, Font J, et al. Outward- and inward-facing structures of a putative bacterial transition-metal transporter with homology to ferroportin. *Nat Commun*. 2015;6(1):8545-8545.

25. Deshpande CN, Ruwe TA, Shawki A, et al. Calcium is an essential cofactor for metal efflux by the ferroportin transporter family. *Nat Commun*. 2018;9(1): 3075.

26. Kaback HR. A chemiosmotic mechanism of symport. *Proc Natl Acad Sci U S A*. 2015;112(5):1259-1264.

27. Guan L, Kaback HR. Lessons from lactose permease. *Annu Rev Biophys Biomol Struct*. 2006;35(1):67-91.

28. Wisedchaisri G, Park MS, Iadanza MG, Zheng H, Gonen T. Proton-coupled sugar transport in the prototypical major facilitator superfamily protein XylE. *Nat Commun*. 2014;5(1):4521.

29. Kelley LA, Mezulis S, Yates CM, Wass MN, Sternberg MJ. The Phyre2 web portal for protein modeling, prediction and analysis. *Nat Protoc*. 2015;10(6): 845-858.

30. Martinez-Finley EJ, Chakraborty S, Fretham SJ, Aschner M. Cellular transport and homeostasis of essential and nonessential metals. *Metallomics*. 2012; 4(7):593-605.

31. Yin Z, Jiang H, Lee ES, et al. Ferroportin is a manganese-responsive protein that decreases manganese cytotoxicity and accumulation. *J Neurochem*. 2010;112(5):1190-1198.

32. Troadec MB, Ward DM, Lo E, Kaplan J, De Domenico I. Induction of FPN1 transcription by MTF-1 reveals a role for ferroportin in transition metal efflux. *Blood*. 2010;116(22):4657-4664.

33. Aydemir F, Jenkitkasemwong S, Gulec S, Knutson MD. Iron loading increases ferroportin heterogeneous nuclear RNA and mRNA levels in murine J774 macrophages. *J Nutr*. 2009;139(3):434-438.

34. Delaby C, Pilard N, Gonçalves AS, Beaumont C, Canonne-Hergaux F. Presence of the iron exporter ferroportin at the plasma membrane of macrophages is enhanced by iron loading and down-regulated by hepcidin. *Blood*. 2005;106(12):3979-3984.

35. Yang F, Wang X, Haile DJ, Piantadosi CA, Ghio AJ. Iron increases expression of iron-export protein MTP1 in lung cells. *Am J Physiol Lung Cell Mol Physiol*. 2002;283(5):L932-L939.

36. Chung J, Haile DJ, Wessling-Resnick M. Copper-induced ferroportin-1 expression in J774 macrophages is associated with increased iron efflux. *Proc Natl Acad Sci U S A*. 2004;101(9):2700-2705.

37. Callebaut I, Joubrel R, Pissard S, et al. Comprehensive functional annotation of 18 missense mutations found in suspected hemochromatosis type 4 patients. *Hum Mol Genet*. 2014;23(17):4479-4490.

38. Schimanski LM, Drakesmith H, Merryweather-Clarke AT, et al. In vitro functional analysis of human ferroportin (FPN) and hemochromatosis-associated FPN mutations. *Blood*. 2005;105(10):4096-4102.

39. Detivaud L, Island ML, Jouanolle AM, et al. Ferroportin diseases: functional studies, a link between genetic and clinical phenotype. *Hum Mutat*. 2013; 34(11):1529-1536.

40. Fernandes A, Preza GC, Phung Y, et al. The molecular basis of hepcidin-resistant hereditary hemochromatosis. *Blood*. 2009;114(2):437-443.

41. Gunshin H, Mackenzie B, Berger UV, et al. Cloning and characterization of a mammalian proton-coupled metal-ion transporter. *Nature*. 1997;388(6641): 482-488.

42. Shawki A, Knight PB, Maliken BD, Niespodzany EJ, Mackenzie B. H(+)-coupled divalent metal-ion transporter-1: functional properties, physiological roles and therapeutics. *Curr Top Membr*. 2012;70:169-214.

43. Thwaites DT, Anderson CMH. H+-coupled nutrient, micronutrient and drug transporters in the mammalian small intestine. *Exp Physiol*. 2007;92(4): 603-619.

44. Andrews NC. Disorders of iron metabolism. *N Engl J Med*. 1999;341(26):1986-1995.

45. Roy A, Kucukural A, Zhang Y. I-TASSER: a unified platform for automated protein structure and function prediction. *Nat Protoc*. 2010;5(4):725-738.